Graphene-Based Patterning and Differentiation of C2C12 Myoblasts

*Piyush Bajaj, Jose A. Rivera, Daniel Marchwiany, Vita Solovyeva, and Rashid Bashir**

With the recent advances in stem cell technology and regenerative medicine, it has become imperative to investigate new materials that could be used to improve the functionality of cells or tissues. In addition to being biocompatible, the material must also possess properties that can be used to control the fate of cells. Graphene, a 2D allotrope of carbon,[1] has drawn much attention because of its unique material characteristics. As a result, graphene has found applications in physics, chemistry, and biology.[2] In biomedicine, graphene has been used for a variety of applications such as drug/gene delivery, photodynamic therapy, biosensors, and conductive scaffolds to name a few.[3–5] Graphene and it derivatives have also been used to study the adhesion, proliferation, and differentiation of a variety of mammalian cells.[6] Recent reports have shown that graphene enhances the differentiation of human mesenchymal stem cells (hMSCs) towards osteogenic lineage while graphene oxide (GO) drives hSMCs towards adipogenic lineage.[7] Park et al.[8] reported that human neural stem cells efficiently differentiated to neurons and not glial cells on graphene. Bendali et al.[9] showed that purified neurons can grow and proliferate on peptide-free graphene surfaces. Chen et al.[10] reported that GO expedited the differentiation of induced pluripotent stem cells towards endodermal lineage while graphene suppressed it.

It can be seen that graphene has been used as a scaffold to control the fate of a variety of cell types. However, biomedical applications of graphene, specifically, those related to muscle tissue engineering have been relatively unexplored. The development of tissue-engineered muscles holds promise for the treatment of a variety of myopathies.[11] Moreover, the ability to grow a large volume of functional skeletal muscle in vitro can offer a potential solution for the replacement of failing tissues and organs.[12,13] In addition, tissue-engineered muscles can also be used as actuators for a variety of microelectromechanical systems (MEMS) and bio-hybrid devices.[14,15]

However, there has been no study to date that investigated the interaction of C2C12 muscle cells on native peptide-free graphene substrates. Recently, Ku and co-workers looked at the proliferation and differentiation of C2C12 myoblasts on derivatives of graphene: GO and reduced GO (rGO).[16] They performed an excellent molecular analysis of the muscle differentiation specific genes (MyoD, myogenin, Troponin T, myosin heavy chain (MHC)) and concluded that myogenic differentiation was enhanced on GO. However, alignment and functionality, the two hallmark properties of mature myotubes, were not explored in this study.[17,18] In addition, graphene and GO can have different cellular responses to the same cell type.[7,10] Since, the molecular aspect of myogenesis has been previously studied on GO, our study aimed at looking at its functional aspect on graphene.

C2C12 skeletal muscle myoblasts were seeded on graphene films. It was found that graphene not only supported the growth of muscle cells but also enhanced their differentiation. By culturing these cells in the media supplemented with insulin-like growth factor (IGF-1), a positive regulator for muscle growth, fusion indices over 70% were recorded. Furthermore, spontaneous myotube alignment was observed in accordance with the underlying lithographically patterned graphene substrate. Finally, to test the functionality of the myotubes, they were stimulated by a custom-built electrical pulse stimulator. Differentiated mature myotubes efficiently responded to these electrical stimulations by actuating at the same rate as the input signal. Our cumulative findings suggest that native graphene can be used to develop artificially engineered functional muscles, which can have applications for the development of bio-hybrid actuators, biological MEMS (BioMEMS), and muscle tissue engineering.

Figure 1A shows the fluorescent images of the cells on graphene and SiO_2 over a period of 4 days in differentiation media (DM) without IGF-1. SiO_2 was chosen as one of the controls in the study since, silicon it is the most commonly used material for microfabrication and MEMS.[19] It can be seen that the percentage of myotubes (green, MHC) increased as a function of time on both graphene and oxide surfaces. However, myotubes were mostly present on graphene with very little myotube formation on the oxide surface. This difference became even more prominent when the DM was supplemented with IGF-1 (Figure 1B). The graphene region of the chip showed a very dense coverage of myotubes as early as day 2 while a sparse coverage was seen on the oxide surface. Figure 1C shows the

Dr. P. Bajaj,[+] J. A. Rivera, Prof. R. Bashir
Department of Bioengineering
University of Illinois at Urbana-Champaign
Urbana, IL 61801, USA
E-mail: rbashir@illinois.edu
Dr. P. Bajaj,[+] J. A. Rivera, D. Marchwiany,
Dr. V. Solovyeva, Prof. R. Bashir
Micro and Nanotechnology Laboratory
University of Illinois at Urbana-Champaign
Urbana, IL 61801, USA
Dr. D. Marchwiany
Department of Molecular and Cellular Biology
University of Illinois at Urbana-Champaign
Urbana, IL 61801, USA
V. Solovyeva, Prof. R. Bashir
Department of Electrical and Computer Engineering
University of Illinois at Urbana-Champaign
Urbana, IL 61801, USA
[+]Present address: Defense Systems and Analysis Division,
Los Alamos National Laboratory, Los Alamos, NM 87544, USA

DOI: 10.1002/adhm.201300550

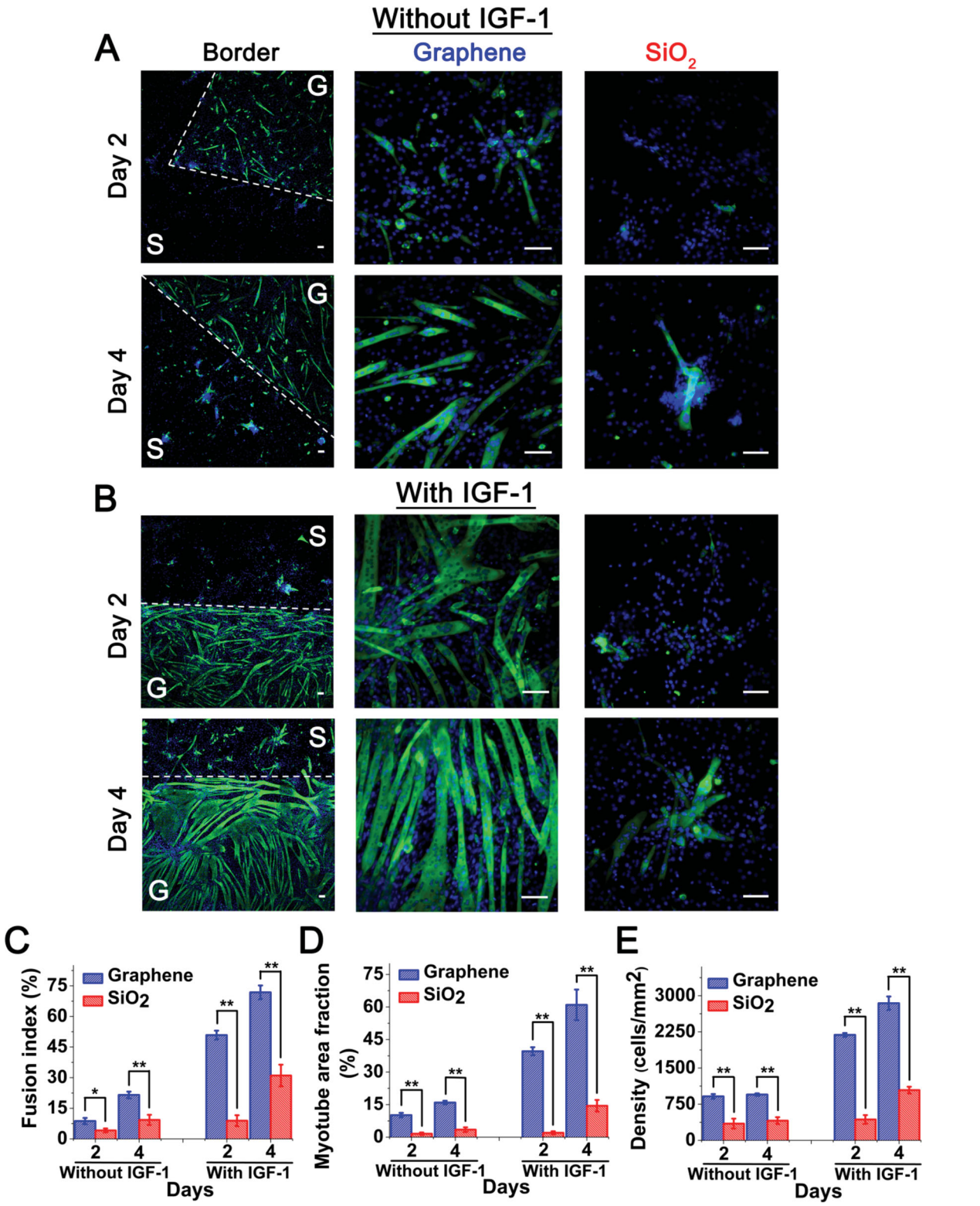

Figure 1. C2C12 cells on graphene (G)/SiO_2 (S) chips in DM with and without IGF-1. A) Without IGF-1. Fluorescent images of the C2C12 cells on graphene and SiO_2. Column 1 shows the cells on the border of graphene and SiO_2 regions of the chip for days 2 and 4. Column 2 shows the cells on graphene and column 3 shows the cells on SiO_2. Row 1 shows the C2C12 cells on day 2, while row 2 shows the cells on day 4. Cells were stained for anti-MHC (green) and nucleus (blue) and these were used for the calculation of the fusion index. The dashed white bar in column one is the border of SiO_2 and graphene surfaces on the chip. Scale bar is 100 µm. B) With IGF-1. Quantification of C) fusion index, D) myotube area fraction, and E) cell density for C2C12 cells on graphene and SiO_2. Significance: $^{**}p < 0.01$ and $^{*}p < 0.05$. Data are represented as mean ± SE ($n = 5$).

fusion index of C2C12 cells on graphene and oxide surfaces. By day 4, graphene showed a fusion index of 21.5% while only 9.3% C2C12 cells fused to form myotubes on the oxide surface for DM without IGF-1. These results were statistically significant at $p < 0.01$. In our previous study, standard tissue culture petri dishes reported fusion indices of 19.9% after 4 d for similar conditions.[17] This shows that the myogenic differentiation potential of C2C12 cells on graphene is comparable to tissue culture dishes. The fusion index showed a striking rise in response to the addition of IGF-1 to the DM. See Figure S1 (Supporting Information) for the effect of IGF-1 on the differentiation potential of C2C12 cells on standard tissue culture petri dishes. Additionally, these tissue culture petri dishes can serve as a second control in the study. For DM supplemented with IGF-1, the fusion index of C2C12 cells quickly rose to 71.8% on graphene, more than twice larger than the oxide surface. Furthermore, it has been previously shown that IGF-1 treated myotubes showed enhanced contractile force generation in vitro.[20] Thus IGF-1-treated C2C12 myotubes on graphene have the potential to restore load bearing muscle function in vivo. Also, these results indicate that graphene-muscle-based MEMS actuators can outperform their silicon-muscle-based counterparts. Recent reports have already shown that graphene-based MEMS offers better sensitivity than commonly used MEMS materials such as silicon and SU8.[21,22]

The myotube area fraction was 15.9% on graphene while only 3.5% was seen on the oxide surface for DM without IGF-1 (Figure 1D). By adding IGF-1 to the media, the myotube area fraction on graphene increased to 60.9%, about four times larger than the oxide surface. This increase in the fusion index and myotube area fraction can be attributed to the higher density of C2C12 cells on graphene versus the oxide surface (Figure 1E). On day 4, graphene showed an average density of 950 cells mm^{-2} while the density was only 408 cells mm^{-2} on the oxide surface for DM without IGF-1. This difference in the cell density was even more prominent with the addition of IGF-1 to the DM. Graphene exhibited almost three times larger density than the oxide surface. The density of cells on graphene after 4 d was even larger than that seen on standard tissue culture petri dishes in 5 d (Figure S1C, Supporting Information). "Community effect" is a well-known phenomenon in C2C12 myogenesis where higher initial cell density increases the differentiation of C2C12 cells.[23] Thus the myogenic potential of C2C12 cells can be summarized as graphene ≥ tissue culture petri dishes >> oxide. In addition, monolayer graphene is optically transparent, electrically conductive, and easily transferrable to a variety of substrates.[24] This makes graphene an ideal biomaterial for muscle tissue engineering and BioMEMS.

The root mean square roughness of graphene obtained from the atomic force microscopy data was 5 nm for a 100 μm^2 scan area (see Figure S2, Supporting Information, for characterization of the graphene films) while that of the oxide surface has been previously shown to be 0.4–0.6 nm.[25,26] The increase in the surface roughness provided higher attachment sites for the cells and possibly increased their migration towards graphene.[27,28] It has been shown that fibroblasts migrated from smooth glass to nanorough glass.[28] Lampin et al. also showed that given the choice between two similar surfaces, cells tend to prefer a slightly rougher surface irrespective of the cell type.[19,29] Furthermore, SiO_2 is very hydrophilic (water contact angle is ≈30°) while the water contact angle of graphene was 79.7° ± 3.3° (measured, $n = 5$), making it moderately hydrophilic.[25,30] The optimum contact angle for attachment of cells is around 64° with a decrease in cell adhesion on very hydrophilic or very hydrophobic surfaces.[27] Bumgardner et al.[31] investigated the influence of contact angle on the attachment of osteoblasts. They showed that chitosan-coated titanium surfaces with a water contact angle of 76.4° resulted in a much higher cell attachment and protein adsorption (fibronectin, albumin) compared to the bare titanium control (water contact angle = 32.2°) . In addition, it is well known that serum protein adsorption on the substrate plays a big role in the attachment properties of cells. Graphene and its derivatives have a high capacity of serum protein adsorption.[7] Since, serum proteins contain a lot of extracellular proteins such as albumin and fibronectin,[32] these proteins can get easily adsorbed on the graphene surfaces. The higher density of these ECM proteins on graphene surfaces results in higher adhesion sites for the cells, which in turn lead to higher cell density on graphene. The π-electrons of graphene could also interact with the hydrophobic core of the deposited proteins, further enhancing the attachment of C2C12 cells.[7] Thus most likely by higher initial C2C12 cell recruitment, graphene enhanced the process of C2C12 myogenesis.

Organized cell alignment is critical to the formation of engineered tissues. In vivo, alignment enhances the functionality of a number of tissues such as muscles, vasculature, and nerves.[33–35] In particular, alignment is extremely important for skeletal and cardiac muscles as it maximizes their contractile power. A number of techniques such as micro-contact printing (μCP), dielectrophoresis, and electrical stimulation have been used to achieve a high degree of cell alignment or patterning.[17,36,37] In this study, alignment and patterning of myotubes were spontaneously achieved as C2C12 cells have a much higher affinity for attachment on graphene than the oxide surface.

Graphene was patterned into 150 μm by 1500 μm rectangular islands using standard photolithography techniques (see Figure S2A,B, Supporting Information, for the fabrication overview on patterning of graphene). **Figure 2**A shows the alignment of C2C12 myotubes on lithographically patterned graphene islands over a period of 4 days. Most of the myotubes formed on graphene islands while very few C2C12 cells differentiated to myotubes on the oxide surface. The nuclear density was also much higher on graphene than the oxide surface. It was interesting to note that even though the oxide surface showed cell attachment and spreading (see Figure S3, Supporting Information, for actin staining of cells), majority of C2C12 differentiation mainly happened on graphene. Figure S4 (Supporting Information) shows the patterning of C2C12 myotubes on a different type of geometry, hybrid 30° patterns. This confirms that myotube patterning on graphene can be achieved on a variety of geometries. Hybrid 30° patterns were chosen because our previous study showed that this geometry maximized the differentiation of C2C12 myoblasts.[17] Figure 2B shows the fast Fourier transform (FFT) alignment plot of the images for the fluorescein isothiocyanate (FITC, green) channel on days 2 and 4. It can be seen that on day 2, myotubes on the top, center, and bottom graphene islands were highly aligned

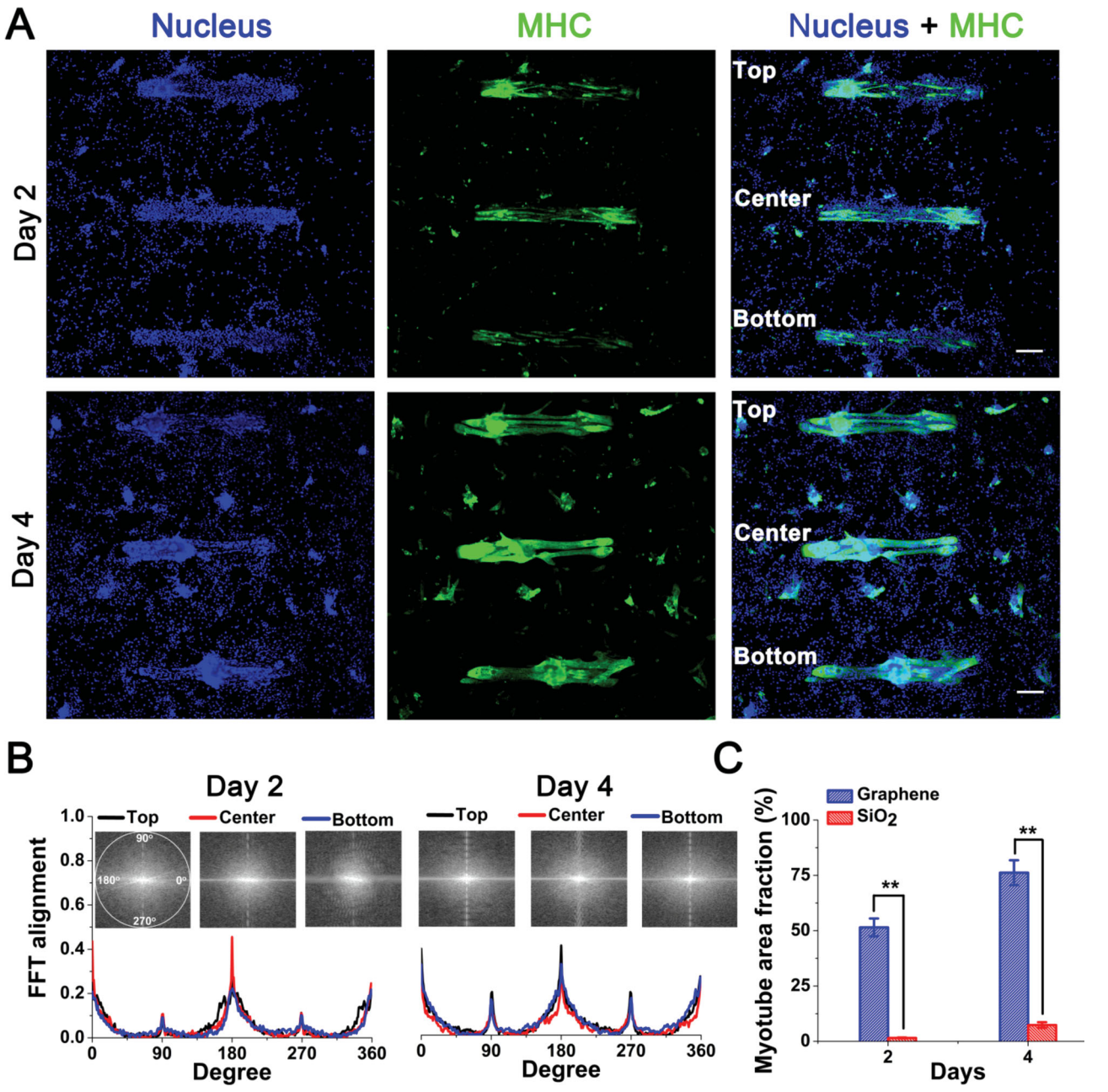

Figure 2. Patterning and alignment of C2C12 myotubes on graphene/SiO_2 chips in DM with IGF-1. A) Fluorescent images of the C2C12 myotubes on lithographically patterned graphene islands. Row 1 shows the C2C12 myotubes on day 2. Row 2 shows the cells on day 4. Column 1 shows the cells stained for nucleus (blue) on graphene and SiO_2 regions of the chip for days 2 and 4. Column 2 shows the cells stained for anti-MHC (green) on graphene and SiO_2 regions of the chip for days 2 and 4. Column 3 shows the merged images by combining columns 1 and 2. The top, center, and bottom correspond to the graphene islands in the merged images. Scale bar is 250 μm. B) Alignment of C2C12 myotubes on graphene islands quantified by FFT alignment plot for days 2 and 4. The FFT alignment plot was obtained from the FFT of the FITC channel images, which are shown in the inset for each of the top, center, and bottom graphene islands. C) Quantification of myotube area fraction for C2C12 cells on graphene and SiO_2. Significance: $^{**}p < 0.01$. Data are represented as mean ± SE ($n = 3$).

as evidenced from the sharp and narrow peaks at 180°. The inset of the figure shows the FFT of the top, center, and bottom graphene islands, respectively. Even on day 4, myotubes on the top, center, and bottom graphene islands showed a good degree of alignment as evidenced from the sharp peak at 180° in the FFT alignment plot. The smaller peaks at 90° and 270° in Figure 2B were most likely the result of edge effects.[36,38] Figure S5 (Supporting Information) shows the FFT alignment plot for the myotubes cultured in a tissue culture petri dish with IGF-1. This is indicative of a sample with very little to no net alignment. Thus by lithographically patterning graphene and using the fact that C2C12 cells preferred graphene

over oxide surface, we were able to achieve a high degree of spontaneous myotube alignment and patterning on graphene. This is the first study that has shown graphene-based spontaneous alignment of myotubes. As cellular/tissue alignment plays a key role for maximizing the contractile power for muscles, this spontaneous alignment of myotubes using graphene can be a very simple approach for patterning muscle tissues in vitro. Figure 2C shows the myotube area fraction on graphene and oxide surfaces of the chip. Over 76% of the graphene area was covered by myotubes while only 7.4% of the oxide surface showed myotube coverage. This big difference in the affinity of C2C12 myotubes to graphene over oxide can be useful for selectively patterning muscles for both in vivo and in vitro applications.

Muscles are electrogenic tissues. In order to show that graphene not only lead to differentiation of muscles but also improved their maturity, it was important to evaluate the functionality of these muscles on graphene surfaces by electrical stimulation. Figure S6 (Supporting Information) shows the custom-designed electrical pulse stimulator that was used for testing the functionality of the myotubes. Electrolysis is a big problem whenever an electrical current is passed through an ionic liquid at low frequencies. It leads to the creation of reactive species, which can be detrimental to the viability of cells.[39] Therefore, a 220 μF capacitor was put in series with the circuit. Thus, even though the generated waveform was a monophasic pulse, the resistor–capacitor (RC) nature of the circuit made it a biphasic pulse. This tremendously minimized electrolysis and allowed the stimulation of myotubes. Myotubes contracted at the same rate at which the frequency pulse was applied from the waveform generator (**Figure 3**, Figure S6, Supporting Information). Quantum dots were used for particle tracking by kymograph as described previously.[17] By applying a frequency of 1 Hz (Figure 3A), the myotubes contracted at 1 Hz (For movies see Supporting Information). The inset of the figure shows the FFT periodogram. The periodogram shows the major frequency component of the kymograph. In addition, as seen in Figure 3B,C, various combinations of frequency (1, 2 Hz or 1, 3, 1 Hz) could also be applied in the same window of time and the myotubes followed that frequency cycle. Twitch responses of cells were seen at lower frequencies while the myotubes went into tetanus at higher frequencies (>15 Hz). This showed that the myotubes on graphene not only showed a high degree of myogenic differentiation but also they were mature and highly functional.

In summary, we have shown that C2C12 cells efficiently differentiate on graphene and this differentiation potential of C2C12 cells was further enhanced by the addition of IGF-1. By patterning graphene islands on oxide surfaces, majority of the myotubes were constricted on these graphene surfaces. This leads to spontaneous alignment of the myotubes. In addition, we also confirmed that the myotubes formed on these graphene surfaces were highly functional and responded efficiently to electrical pulse stimulations. Our cumulative findings suggest that graphene can be used for the development of artificially engineered functional skeletal muscles, BioMEMS, and bio-hybrid actuators.

Experimental Section

Preparation and Patterning of Graphene Films: Graphene was grown by chemical vapor deposition (CVD) method on copper foil (99.8%; Alfa Aesar 0.001 inch) based on previously published protocol.[40] See Supporting Information for the complete description and characterization of CVD grown graphene films.

Cell Culture and Immunofluorescence: C2C12 cells were cultured using standard aseptic tissue culture techniques in media supplemented with 10% fetal bovine serum and 1% antibiotics (growth medium, GM). The graphene/SiO_2 chips were placed in an ultra-low attachment six-well plate and approximately 80 000 C2C12 cells were seeded in each of the wells. To induce differentiation, the cells were starved of serum and cultured in a media with 2% horse serum (DM). All time points in the figure refer to cells being present in DM. At the respective time points, cells were fixed, permeabilized and blocked with 4% paraformaldehyde, 0.2% Triton X-100 and 1% bovine serum albumin respectively. For imaging, cells were incubated with the primary anti-body, MF20 (MHC) overnight at 4 °C and then with the secondary anti-body, goat anti-mouse and 4′,6-diamidino-2-phenylindole for 2 h at 37 °C. For the experiments involving IGF-1, 50 ng mL^{-1} was added to the DM.

Quantitative Analysis: The fusion index was calculated as the ratio of the nuclei number in myocytes with two or more nuclei to the total number of nuclei.[17] The area fraction of myotube was calculated by finding the area of myotubes stained with MHC. Nuclear density was calculated by counting the number of nuclei per unit area of the image. The stained cells were imaged with a fluorescent microscope and the images were quantified using ImageJ. Image alignment was quantified by 2D FFT using ImageJ. For an excellent discussion on FFT-based alignment quantification, the reader is encouraged to read Ayres et al.[38] Statistical analysis was performed using one-way analysis of variance

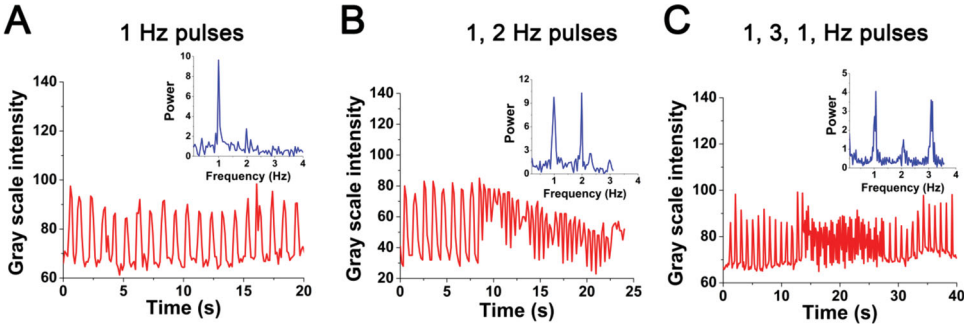

Figure 3. Electrical pulse stimulation of C2C12 myotubes on graphene in DM with IGF-1 on day 4. Myotubes stimulated at different frequencies using the electrical pulse stimulator. A) 1 Hz, B) 1, 2 Hz, C) 1, 3, 1 Hz. The grayscale values from the kymograph are plotted as a function of time. The inset shows the periodogram from the kymograph by FFT.

(ANOVA) and the values reported in the study are mean ± standard error of the mean (SE).

Electrical Stimulation of Myotubes: The cyclic contraction of myotubes was achieved by using a custom-built electrical pulse stimulator, which has been previously described.[17] To actuate the myotubes, an electrical pulse of 15 V, duration 50–100 ms and varying frequency was applied between two platinum electrodes spaced 1 cm apart.

Supporting Information

Supporting Information is available from the Wiley Online Library or from the author.

Acknowledgements

The MHC antibody developed by Dr. Donald A. Fischman was obtained from the Developmental Studies Hybridoma Bank developed under the auspices of the National Institute of Child Health and Development (NICHD) and maintained by The University of Iowa, Department of Biology, Iowa City, IA 52242. This project was made possible by a co-operative agreement that was awarded and administered by the US Army Medical Research & Materiel Command (USAMRMC) and the Telemedicine & Advanced Technology Research Center (TATRC), under Contract #: W81XWH0810701 and National Science Foundation Science and Technology Center "Emergent Behaviors of Integrated Cellular Systems" Grant CBET-0939511.

Received: October 7, 2013
Published online: December 18, 2013

[1] K. S. Novoselov, A. K. Geim, S. V. Morozov, D. Jiang, Y. Zhang, S. V. Dubonos, I. V. Grigorieva, A. A. Firsov, *Science* **2004**, *306*, 666.
[2] S. Z. Butler, S. M. Hollen, L. Cao, Y. Cui, J. A. Gupta, H. R. Gutiérrez, T. F. Heinz, S. S. Hong, J. Huang, A. F. Ismach, E. Johnston-Halperin, M. Kuno, V. V. Plashnitsa, R. D. Robinson, R. S. Ruoff, S. Salahuddin, J. Shan, L. Shi, M. G. Spencer, M. Terrones, W. Windl, J. E. Goldberger, *ACS Nano* **2013**, *7*, 2898.
[3] J. T. Robinson, S. M. Tabakman, Y. Liang, H. Wang, H. Sanchez Casalongue, D. Vinh, H. Dai, *J. Am. Chem. Soc.* **2011**, *133*, 6825.
[4] N. Li, Q. Zhang, S. Gao, Q. Song, R. Huang, L. Wang, L. Liu, J. Dai, M. Tang, G. Cheng, *Sci. Rep.* **2013**, *3*.
[5] L. Z. He Shen, M. Liu, Z. Zhang, *Theranostics* **2012**, *2*, 283.
[6] S. H. Ku, M. Lee, C. B. Park, *Adv. Healthcare Mater.* **2013**, *2*, 244.
[7] W. C. Lee, C. H. Y. X. Lim, H. Shi, L. A. L. Tang, Y. Wang, C. T. Lim, K. P. Loh, *ACS Nano* **2011**, *5*, 7334.
[8] S. Y. Park, J. Park, S. H. Sim, M. G. Sung, K. S. Kim, B. H. Hong, S. Hong, *Adv. Mater.* **2011**, *23*, H263.
[9] A. Bendali, L. H. Hess, M. Seifert, V. Forster, A.-F. Stephan, J. A. Garrido, S. Picaud, *Adv. Healthcare Mater.* **2013**, *2*, 929.
[10] G. Y. Chen, D. W. P. Pang, S. M. Hwang, H. Y. Tuan, Y. C. Hu, *Biomaterials* **2012**, *33*, 418.
[11] C. Favreau, E. Delbarre, J. C. Courvalin, B. Buendia, *Exp. Cell Res.* **2008**, *314*, 1392.
[12] A. D. Bach, J. P. Beier, J. Stern-Staeter, R. E. Horch, *J. Cell. Mol. Med.* **2004**, *8*, 413.
[13] M. Koning, M. C. Harmsen, M. J. A. v. Luyn, P. M. N. Werker, *J. Tissue Eng. Reg. M.* **2009**, *3*, 407.
[14] H. Fujita, V. Dau, K. Shimizu, R. Hatsuda, S. Sugiyama, E. Nagamori, *Biomed. Microdevices* **2011**, *13*, 123.
[15] K. Shimizu, H. Sasaki, H. Hida, H. Fujita, K. Obinata, M. Shikida, E. Nagamori, *Biomed. Microdevices* **2010**, *12*, 247.
[16] S. H. Ku, C. B. Park, *Biomaterials* **2013**, *34*, 2017.
[17] P. Bajaj, B. Reddy, L. Millet, C. Wei, P. Zorlutuna, G. Bao, R. Bashir, *Integr. Biol.* **2011**, *3*, 897.
[18] H. Aubin, J. W. Nichol, C. B. Hutson, H. Bae, A. L. Sieminski, D. M. Cropek, P. Akhyari, A. Khademhosseini, *Biomaterials* **2010**, *31*, 6941.
[19] M. Ni, W. H. Tong, D. Choudhury, N. A. A. Rahim, C. Iliescu, H. Yu, *Int. J. Mol. Sci.* **2009**, *10*, 5411.
[20] M. Sato, A. Ito, Y. Kawabe, E. Nagamori, M. Kamihira, *J. Biosci. Bioeng.* **2011**, *112*, 273.
[21] A. D. Smith, F. Niklaus, A. Paussa, S. Vaziri, A. C. Fischer, M. Sterner, F. Forsberg, A. Delin, D. Esseni, P. Palestri, M. Östling, M. C. Lemme, *Nano Lett.* **2013**, *13*, 3237.
[22] C. Martin-Olmos, H. I. Rasool, B. H. Weiller, J. K. Gimzewski, *ACS Nano* **2013**, *7*, 4164.
[23] G. Messina, C. Blasi, S. A. La Rocca, M. Pompili, A. Calconi, M. Grossi, *Mol. Biol. Cell* **2005**, *16*, 1469.
[24] J. U. Park, S. Nam, M. S. Lee, C. M. Lieber, *Nat. Mater.* **2012**, *11*, 120.
[25] P. Bajaj, D. Akin, A. Gupta, D. Sherman, B. Shi, O. Auciello, R. Bashir, *Biomed. Microdevices* **2007**, *9*, 787.
[26] V. Solovyeva, K. Keller, M. Huth, *Thin Solid Films* **2009**, *517*, 6671.
[27] D. P. Dowling, I. S. Miller, M. Ardhaoui, W. M. Gallagher, *J. Biomater. Appl.* **2011**, *26*, 327.
[28] W. Chen, L. G. Villa-Diaz, Y. Sun, S. Weng, J. K. Kim, R. H. W. Lam, L. Han, R. Fan, P. H. Krebsbach, J. Fu, *ACS Nano* **2012**, *6*, 4094.
[29] M. Lampin, R. Warocquier-Clérout, C. Legris, M. Degrange, M. F. Sigot-Luizard, *J. Biomed. Mater. Res.* **1997**, *36*, 99.
[30] H. E. N'guessan, A. Leh, P. Cox, P. Bahadur, R. Tadmor, P. Patra, R. Vajtai, P. M. Ajayan, P. Wasnik, *Nat. Commun.* **2012**, *3*, 1242.
[31] J. D. Bumgardner, R. Wiser, S. H. Elder, R. Jouett, Y. Yang, J. L. Ong, *J. Biomater. Sci., Polym. Ed.* **2003**, *14*, 1401.
[32] S. Oh, K. S. Brammer, Y. S. J. Li, D. Teng, A. J. Engler, S. Chien, S. Jin, *Proc. Natl. Acad. Sci. USA* **2009**.
[33] C. Y. Chung, H. Bien, E. Entcheva, *J. Cardiovasc. Electr.* **2007**, *18*, 1323.
[34] P. Bajaj, D. Khang, T. J. Webster, *Int. J. Nanomed.* **2006**, *1*, 361.
[35] R. Deumens, G. C. Koopmans, C. G. J. den Bakker, V. Maquet, S. Blacher, W. M. M. Honig, R. Jérôme, J. P. Pirard, H. W. M. Steinbusch, E. A. J. Joosten, *Neuroscience* **2004**, *125*, 591.
[36] P. Bajaj, D. Marchwiany, C. Duarte, R. Bashir, *Adv. Healthcare Mater.* **2013**, *2*, 450.
[37] N. Tandon, B. Goh, A. Marsano, P. H. G. Chao, C. Montouri-Sorrentino, J. Gimble, G. Vunjak-Novakovic, *Engineering in Medicine and Biology Society, Annual International Conference of the IEEE* 3–6 Sept. **2009**.
[38] C. E. Ayres, B. S. Jha, H. Meredith, J. R. Bowman, G. L. Bowlin, S. C. Henderson, D. G. Simpson, *J. Biomater. Sci., Polym. Edn.* **2008**, *19*, 603.
[39] S. V. Puttaswamy, S. Sivashankar, R. J. Chen, C. K. Chin, H. Y. Chang, C. H. Liu, *Biotechnol. J.* **2010**, *5*, 1005.
[40] S. Banerjee, J. Shim, J. Rivera, X. Jin, D. Estrada, V. Solovyeva, X. You, J. Pak, E. Pop, N. Aluru, R. Bashir, *ACS Nano* **2012**, *7*, 834.